ChemComm

COMMUNICATION

View Article Online
View Journal | View Issue

Cite this: *Chem. Commun.*, 2019, 55, 4499

Received 7th March 2019,
Accepted 20th March 2019

DOI: 10.1039/c9cc01874c

rsc.li/chemcomm

Photocontrolled morphological conversion and chiral transfer of a snowflake-like supramolecular assembly based on azobenzene-bridged bis(dibenzo-24-crown-8) and a cholesterol derivative†

Hui-Juan Wang,[a] Heng-Yi Zhang,*[ab] Huang Wu,[a] Xian-Yin Dai,[a] Pei-Yu Li[a] and Yu Liu *[ab]

A snowflake-like supramolecular clockwise-helical assembly was fabricated *via* the host–guest interaction of *trans*-azobenzene-bridged bis(dibenzo-24-crown-8) (*trans*-1) and a cholesterol derivative, while a snowflake-like supramolecular non-helical assembly can be obtained upon complexation of *cis*-1 after UV-irradiation, accompanying the disappearance of circular dichroism signals from the azobenzene zone of 1.

Chiral supramolecular assemblies have been attracting extensive interest due to their controllable structural features, accessible preparation, and potential applications in chiral recognition and separation.[1] In particular, their chirality transfer is expected to be applied for the development of versatile chiral chiroptical switching, chiral catalysis and sensing systems.[2] Cholesterol as a chiral motif and its derivatives are a sort of significant candidate for the construction of chiral supramolecular assemblies and have been widely used as building blocks for chiral supramolecular nanostructures,[1a,3] such as nanofibers,[4] nanotubes,[5] nanorolls,[6] helical ribbons,[7] fluffy globules[8] and nanoflowers.[8] Recently, Zhao *et al.* constructed a manipulated property transfer nanosystem through the coassembly of two cholesterol building blocks,[4a] and a dimension and chirality controllable self-assembly *via* an azobenzene modified cholesterol.[6] On the other hand, the binding or encapsulation of a chiral guest in an achiral cavity has been proved to be an effective method for chirality transfer.[1a] Crown ether has a flexible cavity and can be used to construct various supramolecular assemblies with specific functions. Recently, we constructed some stimuli-responsive supramolecular assemblies using crown ethers, such as a luminescent lanthanide supramolecular assembly tuned by the photoreaction of anthracene,[9] a reversibly photoswitchable supramolecular assembly applied as a photoerasable fluorescent ink,[10] a dual-stimuli reversible lanthanide luminescent molecule[11] and so on. Many cholesterol linked crown ethers were reported due to their applications in catalysis,[12] ion selection,[13] organic gel formation[14] and biology.[15] Some cholesterol-stoppered rotaxanes constructed using crown ethers represented gelation and switchable properties to pH and redox changes.[16] All these cholesterol derivative linked crown ethers only showed the properties of either cholesterol or crown ether, while the host–guest supramolecular chiral system based on cholesterol derivatives was not reported, to the best of our knowledge. Here we introduced a photoresponsive azobenzene-bridged bis(dibenzo-24-crown-8) to a cholesterol derivative that resulted in a macroscopic chirality (nanoscale chirality that could be recognized using a microscope) and chiral transfer from the guest to the host.[1] Interestingly, the chirality at the macroscopic level and the chiral transfer effect are photocontrolled. An illustration of the conversion of chiral/archiral snowflake nanostructures under different light irradiation is shown in Scheme 1.

Brief synthesis routes of azobenzene-bridged bis(dibenzo-24-crown-8) (**1**) and cholesterol modified secondary ammonium

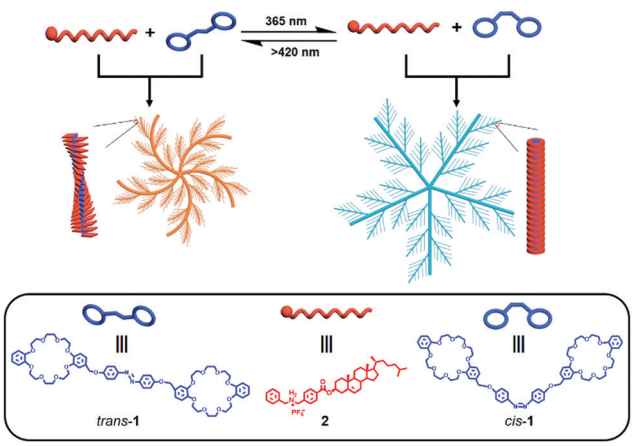

Scheme 1 Schematic representations of **1**, **2** and **2**⊂**1**.

[a] *Department of Chemistry, State Key Laboratory of Elemento-Organic Chemistry, Nankai University, Tianjin 300071, P. R. China. E-mail: hyzhang@nankai.edu.cn, yuliu@nankai.edu.cn*

[b] *Collaborative Innovation Center of Chemical Science and Engineering (Tianjin), Tianjin 300072, China*

† Electronic supplementary information (ESI) available: Detailed synthesis, characterization data, Job's plots, association constants, absorption spectra and transmission electron microscopy images. See DOI: 10.1039/c9cc01874c

salt (**2**) are shown in Scheme S1 (ESI†). Benefiting from the photoisomerism of the azobenzene unit, **1** showed high conversion efficiency and excellent reversibility and repeatability. The *trans–cis* photoisomerization of **1** could be confirmed from the variation in the ultraviolet (UV) absorption spectra upon alternating irradiation with UV and visible light.[17] Generally, the *trans*-isomer of an azobenzene derivative can transform to the *cis*-isomer under irradiation with UV light, and it can reverse back to the *trans*-isomer upon either irradiation with visible light or heating.[18] To quantify the rate of conversion between *trans*-**1** and *cis*-**1**, the irradiation time dependence of the UV absorption spectra for **1** upon irradiation at 365 nm was detected (Fig. S11, ESI†). In dichloromethane, the UV/Vis spectrum of **1** shows a strong π–π* transition at 358 nm and a weak n–π* band near 440 nm, which is the typical absorbance of *trans*-azobenzene. After irradiation with UV light (365 nm) for 15 seconds, the absorption at 358 nm sharply decreased, a stronger n–π* transition arose at 450 nm and weaker bands arose at 310 nm and 277 nm which are the typical absorbance of the *cis*-azobenzene.[19] As can be seen in Fig. 1a, the colour of **1** changed from light yellow to orange after irradiation with UV light (365 nm) for 15 seconds, which was ascribed to the *trans*-isomer that transformed to the *cis*-isomer accompanied by the new absorption peak arising at 450 nm. It is also interesting to further investigate the repetitiveness of the photoisomerism of **1**. As shown in Fig. 1b, the absorption of *trans*-**1** at 358 nm, the characteristic absorption of the π–π* transition of *trans* azobenzene, markedly decreased under light irradiation at 365 nm for 15 seconds, indicating photo isomerization of **1** from *trans* to *cis*. After irradiation with visible light (>420 nm) for 2 seconds, the absorption at 358 nm was recovered, suggesting reverse photoisomerization from *cis* to *trans*. Significantly, this cycle could be completely repeated ten times without any fatigue (Fig. 1b), indicating the good reversibility and repetitiveness of **1**.

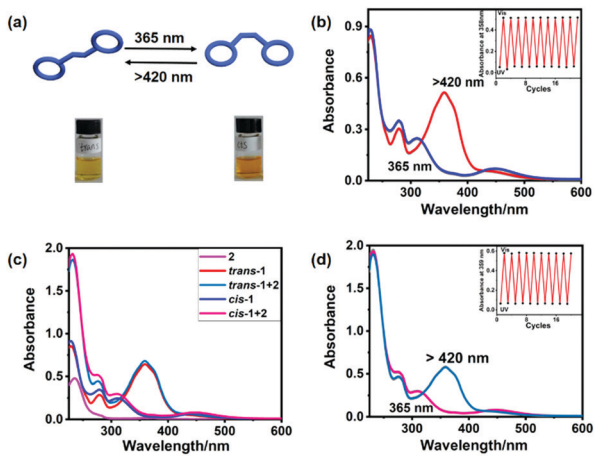

Fig. 1 (a) Chemical structures and changes shown in the photographic images of **1** upon alternating UV and visible light irradiation, (b) UV/Vis spectra of **1** and (inset) absorption changes at 358 nm under irradiation with UV light (365 nm) and visible light (>420 nm). ([**1**] = 3 × 10^{-5} M), (c) UV/Vis spectra of **2**, *trans*-**1**, *cis*-**1**, and **2**⊂*trans*-**1** and **2**⊂*cis*-**1**. ([**1**] = [**2**] = 3 × 10^{-5} M), and (d) UV/Vis spectra of the **2**⊂**1** assembly and (inset) absorption changes at 359 nm under irradiation with UV light (365 nm) and visible light (>420 nm). ([**1**] = 3 × 10^{-5} M, **1**:**2** = 1:2). All samples were prepared in CH_2Cl_2 at 298 K.

^{1}H NMR experiments were performed in $CDCl_3$ to investigate the isomerization efficiency of **1**. After irradiation with 365 nm light for 50 minutes, **1** reached another photostationary state and a series of new signals appeared in the ^{1}H NMR spectrum. As shown in Fig. S12 (ESI†), the protons (H_a, H_b and H_C) of the azobenzene moieties showed obvious upfield shifts ($\Delta\delta$ = 0.10–0.94 ppm). Also the aromatic protons (H_d) of the dibenzo-24-crown-8 moieties showed appreciable upfield shifts ($\Delta\delta$ = 0.10 ppm). The integral of the proton signals indicated that the isomerization efficiency of *trans*-**1** to *cis*-**1** upon irradiation at 365 nm light is 95%. Then after irradiation with visible light (>420 nm) for 30 minutes, **1** reaches another photostationary state (*trans*-**1**). The isomerization efficiency of *cis*-**1** to *trans*-**1** upon irradiation with visible light (>420 nm) is 89%, which is calculated by the integral of the proton signals. Subsequently, after being placed in the dark for one day the resulting isomerized solution transforms back to the initial state. The ^{1}H NMR results further confirm the high conversion efficiency, excellent reversibility and repeatability for **1**. Further, direct morphological information of **1** was investigated by transmission electron microscopy (TEM), scanning electron microscopy (SEM) and dynamic light scattering (DLS). The TEM and SEM images in Fig. 2 and Fig. S14 (ESI†) show that the aggregation of both *trans*-**1** and *cis*-**1** formed nanoparticles. And, the DLS data showed that *trans*-**1** in CH_2Cl_2 solution form nanoparticles with an average hydrodynamic diameter of about 412 nm, while *cis*-**1** is about 458 nm with the same morphology (Fig. S14c and d, ESI†).

The properties of **2** were investigated by UV/Vis, circular dichroism (CD), TEM and SEM studies. As shown in Fig. 3c, the UV spectrum of **2** showed a sharp peak at 238 nm which was assigned to the cholesterol moiety. As expected, an intense Cotton effect appeared at the absorption region of **2**. It is ascribed to the intrinsic molecular chirality of cholesterol units. From the TEM and SEM images of the self-assembly of **2** (Fig. 2c and d), the morphological information revealed a shuttle-like nanosheet. As illustrated in Scheme S2 (ESI†), the model of the molecular arrangement was estimated based on the hydrophobic cholesterol tail and the hydrophilic secondary ammonium salt head. Combining the properties of **2**, we can reasonably deduce that the formation of the nanosheet is ascribed to the intermolecular hydrogen binding and π–π stacking.

It is well documented that the secondary alkylammonium ion noncovalently associates with dibenzo-24-crown-8 through cooperative N–H···O and C–H···O hydrogen-bonding interactions.[20] The assembly behaviors of **1** and **2** were investigated from the UV/Vis, TEM, SEM and CDspectra. Upon the addition of different volumes of **2** to the solution of **1**, the absorption peak of **1** at 277 nm and 358 nm gradually increased (Fig. S13, ESI†). The binding constant was calculated to be 13 400 ± 700 M^{-1} for the association of **1** and **2**. To investigate the photo responsiveness of the assembly of **1** and **2**, the UV/Vis spectra of free **1**, **2** and the **2**⊂**1** assembly irradiated with alternating UV/Vis light were detected. Compared to that of free *trans*-**1** and *cis*-**1**, the

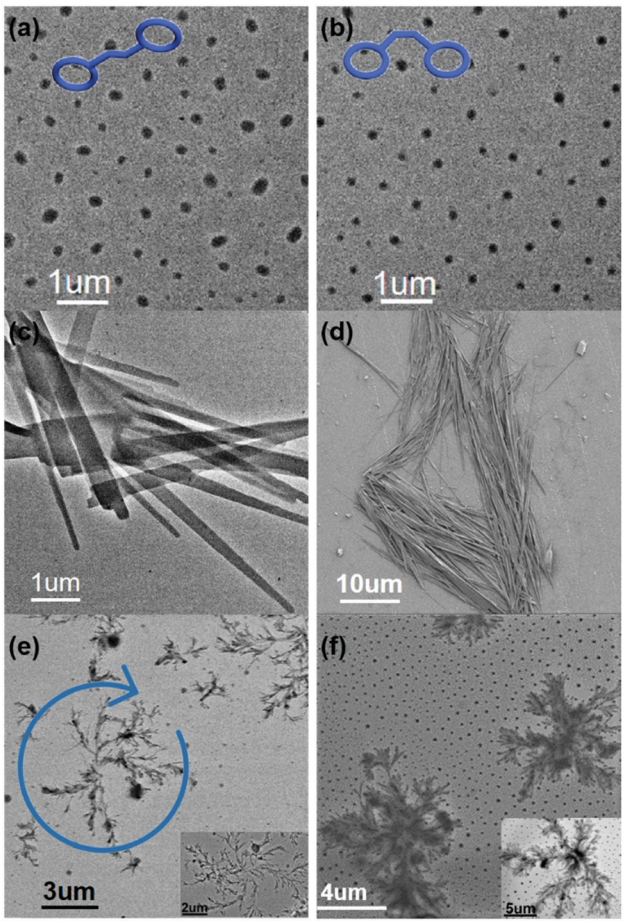

Fig. 2 TEM images and schematic representations (inset) of (a) *trans*-**1**, (b) *cis*-**1** (made by *trans*-**1** upon irradiation with UV light (365 nm) for 50 min ([**1**] = 3.3 × 10^{-4} M)), (c) TEM image of **2**, (d) SEM image of **2**, ([**2**] = 6.6 × 10^{-4} M), and TEM images of (e) **2**⊂*trans*-**1** and (f) **2**⊂*cis*-**1** (made by **2**⊂*trans*-**1** upon irradiation with UV light (365 nm) for 50 min (**1** : **2** = 1 : 2, [**1**] = 3.3 × 10^{-4} M)), all samples were prepared in CH_2Cl_2 at 298 K.

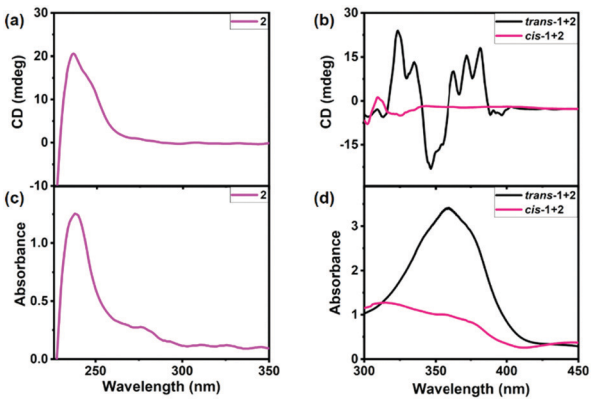

Fig. 3 Circular dichroism spectra of (a) **2** ([**2**] = 10^{-4} M) and (b) **2**⊂*trans*-**1** and **2**⊂*cis*-**1** (**1** : **2** = 1 : 2, [**1**] = 2 × 10^{-3} M). UV/Vis spectra of (c) **2** ([**2**] = 10^{-4} M) and (d) **2**⊂*trans*-**1** and **2**⊂*cis*-**1** (**1** : **2** = 1 : 2, [**1**] = 10^{-4} M) in CH_2Cl_2 at 298 K.

absorption of both **2**⊂*trans*-**1** and **2**⊂*cis*-**1** showed a slight blue shift from 280 nm to 276 nm (Fig. 1c). As expected, the assembly also showed good photocontrolled reversibility and repetitiveness. As shown in Fig. 1d, after being irradiated with UV light (365 nm), the absorption of **2**⊂**1** at 358 nm and 276 nm decreased obviously, and a new peak appeared at 310 nm. Subsequently the sample was irradiated with visible light (>420 nm), and the decreased intensity at 358 nm was recovered to its original level. This could be ascribed to the assembly **2**⊂*cis*-**1** transforming back to the **2**⊂*trans*-**1** assembly (Scheme 1). This experiment was re-performed ten times without any fatigue. In other words, the absorption curves of **2**⊂**1** upon irradiation with alternating UV/Vis light completely overlapped with each other (Fig. 1d).

As per the CD studies, both *trans*-**1** and *cis*-**1** showed a silent Cotton effect at their UV-absorption region, and **2** presented an obvious positive Cotton effect at its UV-Vis absorption region (228–275 nm) (Fig. 3a and c). Interestingly, upon the assembly of *trans*-**1** and **2**, an obvious Cotton effect appeared at the region of 300–400 nm assigned to the absorption of *trans*-**1** (Fig. 3b and d). After irradiation with UV light (365 nm), the CD spectrum of **2**⊂*cis*-**1** showed no obvious Cotton effect in the wavelength of 300–400 nm. Further, we performed several cycles and all of them showed a similar phenomenon. The CD results indicate that the chirality was transferred from **2** to **1**, which could be controlled reversibly and repeatedly by light. More interestingly, the **2**⊂**1** supramolecular assembly exhibited a significantly different assembling behaviour from the free *trans*-**1** or free **2**. The photocontrolled chiral transfer for **2**⊂*trans*-**1** was also confirmed by the observations from TEM and SEM (Fig. 2e and f). In the TEM and SEM images of **2**⊂*trans*-**1**, a number of clockwise rotary snowflake-like nanostructures are shown (Fig. S15, ESI†). The magnified TEM images displayed clear clockwise rotary snowflake-like nanostructures, indicating their helical properties. However, after irradiation with UV light the configuration transferred from **2**⊂*trans*-**1** to **2**⊂*cis*-**1** and its TEM images showed straight stretched non-helical snowflake-like nanostructures bigger than that of **2**⊂*trans*-**1** in size. The system can be switched back with visible light (>420 nm) and the cycle is repeatable. The chirality of **2**⊂**1** observed by TEM and SEM is consistent with the CD results. These phenomena jointly indicate the good reversibility of photocontrolled chirality transfer and the helical/non-helical nanostructure morphological conversion. The strong noncovalent interactions between **1** and **2** enable effective chiral transfer from **2** to *trans*-**1** *via* the host–guest interaction which is different from the classical majority rule. And the chirality transfer was detected on two levels (supramolecular and nanoscopic). Combining these observations, we can reasonably deduce that the snowflake-like morphology is due to the secondary assembly of **2**⊂**1** and the hydrophobic alkyl chains of **2** are exposed to the outer surface. As illustrated in Scheme 2, mainly through the noncovalent interaction and hydrophobic interaction between **1** and **2**, the assembly of **2**⊂**1** presented a snowflake-like conformation. The assembly of **2**⊂*trans*-**1** showed a clockwise rotary snowflake-like nanostructure which was mainly due to the twisting of **2** mediated by *trans*-azobenzene. However, once the assembly of **2**⊂**1** was irradiated with UV light, it isomerized to **2**⊂*cis*-**1**, and presented a non-helical snowflake-like nanostructure which can be ascribed to the opposite twisting behavior of the two cholesterol units mediated by *cis*-azobenzene.

In summary, a snowflake-like supramolecular clockwise-helical assembly has been constructed through the intermolecular

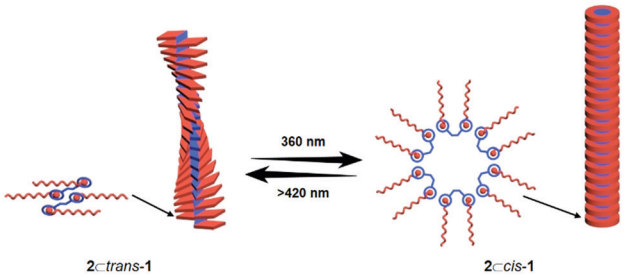

Scheme 2 Schematic representations of the assembly based on the photo-responsive interconversion of **2**⊂*trans*-**1** and **2**⊂*cis*-**1**.

complexation of *trans*-**1** with a cholesterol derivative **2**. After *trans*-**1** in this supramolecular assembly was changed into *cis*-**1** *via* UV irradiation, its helix was lost accompanying the disappearance of CD signals in the azobenzene zone of **1**. The photocontrolled conversion of morphology, transferred chirality and facile preparation properties will endow the supramolecular assembly with potential for application in materials, photo driven chiral switches and information storage.

We thank the National Natural Science Foundation of China (No. 21772100 and 21432004) and the 973 Program (2015CB856500) for financial support.

Conflicts of interest

There are no conflicts to declare.

Notes and references

1 (*a*) M. H. Liu, L. Zhang and T. Y. Wang, *Chem. Rev.*, 2015, **115**, 7304–7397; (*b*) G. A. Hembury, V. V. Borovkov and Y. Inoue, *Chem. Rev.*, 2008, **108**, 1–73; (*c*) P. Xing and Y. Zhao, *Acc. Chem. Res.*, 2018, **51**, 2324–2334.
2 (*a*) G. Liu, J. Liu, C. Feng and Y. Zhao, *Chem. Sci.*, 2017, **8**, 1769–1775; (*b*) F. Wang and C.-L. Feng, *Chem. – Eur. J.*, 2018, **24**, 1509; (*c*) E. Yashima, N. Ousaka, D. Taura, K. Shimomura, T. Ikai and K. Maeda, *Chem. Rev.*, 2016, **116**, 13752–13990; (*d*) L. Mutihac, J. H. Lee, J. S. Kim and J. Vicens, *Chem. Soc. Rev.*, 2011, **40**, 2777–2796.
3 S. S. Badu, V. K. Praveen and A. Ajayaghosh, *Chem. Rev.*, 2014, **114**, 1973–2129.
4 (*a*) P. Xing, H. P. Tham, P. Li, H. Chen, H. Xiang and Y. Zhao, *Adv. Sci.*, 2018, **5**, 1700552; (*b*) P. Xing, Y. Li, Y. Wang, P.-Z. Li, H. Chen, S. Z. F. Phua and Y. Zhao, *Angew. Chem., Int. Ed.*, 2018, **57**, 7774.
5 J. H. Jung, J. A. Rim, S. J. Lee, S. J. Cho, S. Y. Cho, S. Y. Kim, J. K. Kang, Y. M. Kim and Y. J. Kim, *J. Phys. Chem.*, 2007, **111**, 2679–2682.
6 G. Liu, J. Sheng, W. Teo, G. Yang, Y. Li and Y. Zhao, *J. Am. Chem. Soc.*, 2018, **140**, 16275–16283.
7 J. H. Jung, H. Kobayashi, M. Masuda, T. Shimizu and S. Shinkai, *J. Am. Chem. Soc.*, 2001, **123**, 8785–8789.
8 J. H. Jung, Y. Ono, K. Sakurai, M. Sano and S. Shinkai, *J. Am. Chem. Soc.*, 2000, **122**, 8648–8653.
9 Y. Zhou, H.-Y. Zhang, Z.-Y. Zhang and Y. Liu, *J. Am. Chem. Soc.*, 2017, **139**, 7168–7171.
10 H. Wu, Y. Chen and Y. Liu, *Adv. Mater.*, 2017, **29**, 1605271.
11 H.-B. Cheng, H.-Y. Zhang and Y. Liu, *J. Am. Chem. Soc.*, 2013, **135**, 10190–10193.
12 I. K. Sakodinskaya and A. D. Ryabov, *Biotechnol. Lett.*, 2000, **22**, 173–176.
13 Z. H. Sun, M. Barboiu, Y.-M. Legrand, E. Petit and A. Rotaru, *Angew. Chem., Int. Ed.*, 2015, **54**, 14473–14477.
14 (*a*) J. H. Jung, Y. Ono and S. Shinkai, *Tetrahedron Lett.*, 1999, **40**, 8395–8399; (*b*) J. H. Jung, Y. Ono, K. Sakurai, M. Sano and S. Shinkai, *J. Am. Chem. Soc.*, 2000, **122**, 8648–8653.
15 A. Sewbalas, R. U. Islam, W. A. L. van Otterlo, C. B. de Koning, M. Singh, P. Arbuthnot and M. Ariatti, *Med. Chem. Res.*, 2013, **22**, 2561–2569.
16 (*a*) Y. Zhao, I. Aprahamian, A. Trabolsi, N. Erina and J. F. Stoddart, *J. Am. Chem. Soc.*, 2008, **130**, 6348–6350; (*b*) M. Berg, S. Nozinovic, M. Engeser and A. Lützen, *Eur. J. Org. Chem.*, 2015, 5966–5978.
17 K. Atsushi, N. Osamu, K. Tisto, T. Motowo, K. Koji and S. Seiji, *Chem. Lett.*, 1983, 1327–1330.
18 W. Zhang, Y. Chen, J. Yu, X.-J. Zhang and Y. Liu, *Chem. Commun.*, 2016, **52**, 14274–14277.
19 A. A. Beharry and G. A. Woolley, *Chem. Soc. Rev.*, 2011, **40**, 4422–4437.
20 P. R. Ashton, P. J. Cambell, P. T. Glink, D. Philp, N. Spencer, J. F. Stoddart, E. J. T. Chrystal, S. Menzer, D. J. Williams and P. A. Tasker, *Angew. Chem., Int. Ed.*, 1995, **34**, 1865–1869.